Model of orbital populations for voltage-controlled magnetic anisotropy in transition-metal thin films

Jia Zhang,[1,2,*] Pavel V. Lukashev,[3] Sitaram S. Jaswal,[1] and Evgeny Y. Tsymbal[1,*]

[1]*Department of Physics and Astronomy & Nebraska Center for Materials and Nanoscience, University of Nebraska, Lincoln, Nebraska 68588, USA*

[2]*School of Physics & Wuhan National High Magnetic Field Center, Huazhong University of Science and Technology, Wuhan 430074, China*

[3]*Department of Physics, University of Northern Iowa, Cedar Falls, Iowa 50614, USA*

(Received 26 March 2017; revised manuscript received 31 May 2017; published 28 July 2017)

Voltage-controlled magnetic anisotropy (VCMA) is an efficient way to manipulate the magnetization states in nanomagnets and is promising for low-power spintronic applications. The underlying physical mechanism for VCMA is known to involve a change in the *d* orbital occupation on the transition-metal interface atoms with an applied electric field. However, a simple qualitative picture of how this occupation controls the magnetocrystalline anisotropy (MCA) and even why in certain cases the MCA has the opposite sign remains elusive. In this paper, we exploit a simple model of orbital populations to elucidate a number of features typical for the interface MCA, and the effect of the electric field on it, for 3*d* transition-metal thin films used in magnetic tunnel junctions. We find that in all considered cases, including the Fe(001) surface, clean $Fe_{1-x}Co_x$(001)/MgO interface, and oxidized Fe(001)/MgO interface, the effects of alloying and the electric field enhance the MCA energy with electron depletion, which is largely explained by the occupancy of the minority-spin $d_{xz,yz}$ orbitals. However, the hole-doped Fe(001) exhibits an inverse VCMA in which the MCA enhancement is achieved when electrons are accumulated at the Fe (001)/MgO interface with the applied electric field. In this regime, we predict a significantly enhanced VCMA that exceeds 1 pJ/Vm. Realizing this regime experimentally may be favorable for the practical purpose of voltage-driven magnetization reversal.

DOI: 10.1103/PhysRevB.96.014435

I. INTRODUCTION

Magnetocrystalline anisotropy (MCA) is one of the critical parameters that determines the magnetization orientation, switching dynamics, and thermal stability of magnetic media. Ferromagnetic thin films with high magnetic anisotropy promise an easier operation scheme and higher signal stability. However, the larger coercivity of these materials requires high electric currents either to generate a magnetic field or to produce a spin-transfer torque to write the bit information, which imposes significant limitations on their application in portable and high-speed electronic devices. For example, in MgO-based magnetic tunnel junctions (MTJs), which are used in magnetic random access memories (MRAMs), current densities as large as 10^6 A/cm^2 are required to reverse the magnetization of the magnetic bit by spin-transfer torque.

A possible approach to overcome this limitation is to use an electric field, rather than an electric current, to control the magnetization of a ferromagnet [1]. Along these lines, voltage-controlled magnetic anisotropy (VCMA) is considered one of the most promising approaches to dramatically reduce the writing energy of MRAMs [2]. However, a large VCMA effect (∼1 pJ/Vm) is required for device application to overcome large coercivity of the ferromagnetic film, which is needed for its thermal stability.

The effect of an electric field on the surface (interface) magnetic anisotropy has been extensively studied both theoretically [3–15] and experimentally [16–27]. Very large changes in magnetic anisotropy (VCMA ∼ 5 pJ/Vm) were observed due to ionic motion and chemical reactions driven by applied voltage [27,28]. However, ionic motion is a slow process and can hardly be used for device applications in which ultrafast switching of magnetization is required. However, if the VCMA is caused purely by electronic effects, the timescale of the VCMA would lie on subnanosecond regime desirable for applications. It is known that VCMA in Fe(Co)/MgO-based MTJs is largely controlled by the effect of the electric field screening on the ferromagnetic metal surface (interface), resulting in electron doping induced by an external electric field [3].

The main driving mechanism for VCMA is a change in the 3*d* orbital occupation on the transition-metal interface atoms with an applied electric field. Theoretical calculations are capable to predict reasonably well electric field-induced changes in the surface magnetocrystalline anisotropy energy (MAE). However, an intuitive picture for VCMA is missing, even though such a qualitative picture would be helpful for the experimentalists in designing materials and interface structures with enhanced VCMA.

In this paper, we consider a simple model that allows us to qualitatively explain the surface (interface) magnetic anisotropy and the effect of the electric field on it for 3*d* transition-metal thin films used in MTJs. We, first, provide a qualitative picture explaining the expected changes in the MAE as a function of band filling. Then, we perform first principles density functional theory (DFT) calculations to elucidate the effects of the electric field and doping on MAE for a number of Fe-based interfaces, such as Fe(001)/vacuum, $Fe_{1-x}Co_x$(001)/MgO, and Fe(001)/FeO/MgO. We find that the results of these calculations can be reliably explained in terms of changes in the population of the minority-spin $d_{xz,yz}$ orbitals and are qualitatively consistent with the simple model. We predict a sign change and a significant enhancement

*Corresponding authors: jiazhang@hust.edu.cn; tsymbal@unl.edu

of VCMA for the hole-doped Fe(001) interfaces, where it is possible to achieve a record VCMA exceeding 1 pJ/Vm.

II. A SIMPLE MODEL

The microscopic origin of MCA is the relativistic spin-orbital coupling (SOC) $\xi \mathbf{L} \cdot \mathbf{S}$, where $\mathbf{L}$ and $\mathbf{S}$ are the orbital and spin momentum operators, respectively, and ξ is the SOC constant. For films that are not too thick, the largest contribution to MCA comes from surfaces or interfaces due to the reduced symmetry. The surface (interface) MAE is known to be sensitive to the local environment and details of the electronic band structure.

For $3d$ transition-metal films, the MAE can be evaluated using the second-order perturbation theory [29,30], which is applicable due to the relatively small SOC constant ξ (typically in the range of 10–100 meV per atom) compared to the band energies, the crystal field splitting, and the exchange coupling. We define the MAE as the energy difference between the magnetization pointing along the x direction in the plane of the film and the z direction perpendicular to the plane, so that the positive MAE implies the out-of-plane easy axis, known as perpendicular magnetic anisotropy (PMA). In general, the expression for MAE includes both spin-diagonal and spin-nondiagonal matrix elements of the $\mathbf{L} \cdot \mathbf{S}$ term. The exchange splitting in our Fe-based systems is sufficiently large, and the majority-spin band is nearly fully occupied, as shown later in Fig. 3(a), so the dominant contribution to the MAE can be attributed to the minority-spin states. We neglect the contribution from spin-up occupied and spin-down unoccupied states for the qualitative analysis carried out in this paper. Within second-order perturbation theory, the MAE is determined by the matrix elements of SOC between occupied and unoccupied states:

$$E_{\mathrm{MCA}} = \frac{\xi^2}{4} \sum_{o,u} \frac{|\langle \psi_o | L_z | \psi_u \rangle|^2 - |\langle \psi_o | L_x | \psi_u \rangle|^2}{\varepsilon_u - \varepsilon_o}, \quad (1)$$

where ψ_o and ψ_u are unperturbed wave functions for occupied and unoccupied states with energies ε_o and ε_u, respectively.

For transition-metal ferromagnets, such as body-centered cubic (bcc) Fe, the MAE is determined by the energy bands formed from the $3d$ orbitals and depends on their occupations. The crystal field of cubic symmetry splits five d orbitals into the E_g doublet and the T_{2g} triplet, as shown in Fig. 1(a). At the (001) interface, the crystal field symmetry is reduced to tetragonal, which further splits these levels: E_g into two singlets $A_1(d_{z^2})$ and $B_1(d_{x^2-y^2})$ and T_{2g} into singlet $B_2(d_{xy})$ and doublet $E(d_{xz},d_{yz})$. Figure 1(a) shows schematically the orbital order as a function of the energy typical for the Fe/MgO (001) interface.

The dashed red line ($\Delta = D, \delta = 0$) in Fig. 1(b) shows the MAE as a function of orbital filling n in Fig. 1(a). Here, we assume that the number of electrons n can change continuously, reflecting a possibility of additional (noninteger) charge resulting from alloying or the electric field. It is seen that first, the MAE is growing (linearly) due to the population of the d_{xy} orbitals, resulting in a positive contribution to MAE in Eq. (1) through the $\langle d_{xy}|L_z|d_{x^2-y^2}\rangle$ matrix element. Then, it goes down and becomes negative due to the negative

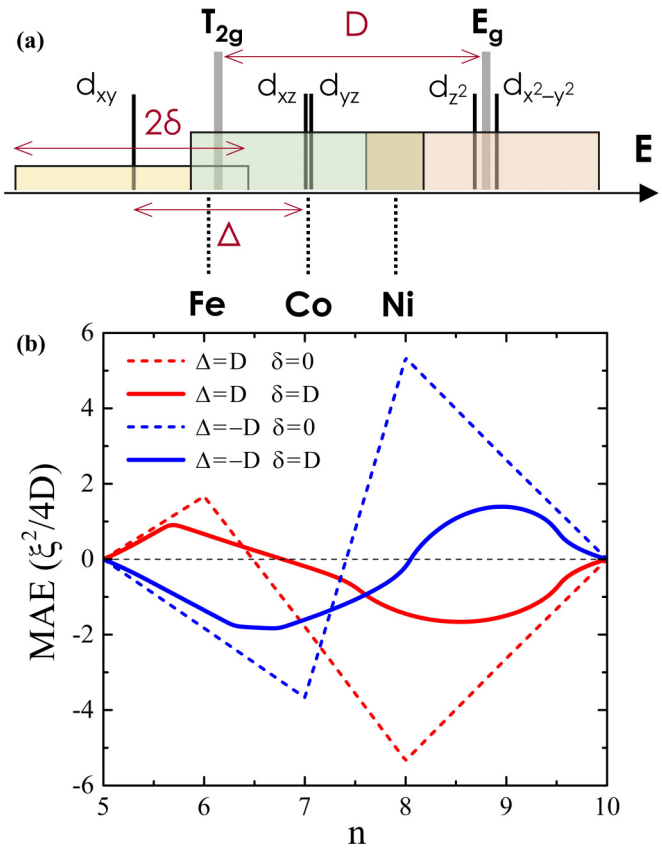

FIG. 1. (a) Schematic of the minority $3d$ orbital splitting by the crystal field of tetragonal symmetry. Broadening of the orbital levels mimics the energy bands. The vertical black dotted lines represent the Fermi energies of Fe, Co, and Ni. (b) MAE as a function of orbital band filling n for different values of the T_{2g} level splitting Δ and broadening δ.

contribution from the d_{yz} orbitals [31] through the matrix elements $\langle d_{yz}|L_x|d_{z^2}\rangle$ and $\langle d_{yz}|L_x|d_{x^2-y^2}\rangle$. Finally, the MAE grows again due to filling of the E_g states, reducing the latter contribution.

Broadening of the orbital states mimics the energy bands, as indicated in Fig. 1(a). Here, for simplicity, we assume a constant density of states (DOS) $\rho_\mu(\varepsilon)$ spread over the energy range from $-\delta/2$ to $+\delta/2$ around the atomic orbital states denoted by index μ. Taking into account that the orbital character is preserved within each broadened level and replacing summation over the occupied and unoccupied states in Eq. (1) by integration, we obtain:

$$E_{\mathrm{MCA}} = \frac{\xi^2}{4} \sum_{\mu,\mu'} P_{\mu\mu'} \int_{-\infty}^{\varepsilon_F} d\varepsilon \int_{\varepsilon_F}^{\infty} d\varepsilon' \frac{\rho_\mu(\varepsilon)\rho_{\mu'}(\varepsilon')}{\varepsilon' - \varepsilon}, \quad (2)$$

where $P_{\mu\mu'} = |\langle \mu | L_z | \mu' \rangle|^2 - |\langle \mu | L_x | \mu' \rangle|^2$ and ε_F is the Fermi energy. The result for $\Delta = D$ is shown in Fig. 1(b) by the solid red line. It is seen that the broadening of the atomic orbitals diminishes the sharp features of MAE versus band filling but preserves its qualitative behavior. The changing sign of $\Delta(\Delta = -D)$ flips the sign of MAE around $n = 6$, as seen from the blue curves in Fig. 1(b).

In a crystalline system with translational symmetry, only transitions between states with the same wave vector **k** are allowed in Eq. (1), making the interpretation more complicated. However, as we will see in Sec. IV, the qualitative features of the VCMA are largely captured within this simple atomiclike picture.

III. DFT CALCULATIONS

The DFT calculations are performed using the projector-augmented wave (PAW) method [32], implemented in the Vienna *Ab initio* Simulation Package (VASP) [33] within the generalized gradient approximation (GGA) for the exchange-correlation potential [34]. The integration method [35] with a 0.05 eV width of smearing is used, along with a plane-wave cutoff energy of 500 eV and convergence criteria of 10^{-4} eV for ionic relaxations and 10^{-3} meV for the total energy calculations. For all considered systems, we use the experimental in-plane lattice constant of bcc Fe, $a = 0.287$ nm. The structures are relaxed in the absence of the electric field until the largest force becomes less than 5.0 meV/Å [36]. Summation over k points is performed using a $24 \times 24 \times 1$ mesh in the first Brillouin zone, which according to our tests is sufficient to provide calculated MAE accuracy of about 0.01 meV.

The MAE is calculated as the difference of total energies calculated self-consistently for the magnetization pointing along the x and z directions in the presence of SOC using VASP [37]. The site- and orbital-projected contributions to the MAE are obtained from the expectation values of the SOC $E_{\mathrm{SOC}} = \langle \frac{\hbar^2}{2m^2c^2} \frac{1}{r} \frac{dV}{dr} \boldsymbol{L} \cdot \boldsymbol{S} \rangle$, where $V(r)$ is the spherical part of the effective potential within the PAW sphere and $\boldsymbol{L}$ and $\boldsymbol{S}$ are orbital and spin operators, respectively. These expectation values are twice the actual values of the total energy correction to the second order in SOC [38]. The second-order perturbation theory is a reasonable approximation for our system, as is evident from the good agreement (with a few percent accuracy) between the total values of MAE obtained from the projected data and the total energy calculations.

For the Fe(001)/MgO interface, in our calculation we use a MgO (4 ML)/Fe (9 ML)/MgO (4 ML)/vacuum (2 nm) supercell [Fig. 2(a)]. The electric field is introduced using the dipole layer placed in the vacuum region of the supercell [39]. The positive electric field is defined as pointing away from the Fe layer to MgO. In this geometry, we can evaluate effects of both positive and negative electric fields by performing calculations for only one direction of the field and evaluating the layer-resolved contribution to the MAE at the two Fe/MgO interfaces. Typically, one or two interfacial monolayers of the ferromagnetic metal provide the dominant contribution to the MAE and VCMA due to short-range electrostatic screening [Figs. 2(b) and 2(c)]. In the oxidized Fe(001)/MgO interface, we assume an additional oxygen atom, which is placed in the first interfacial Fe monolayer atop the interfacial Mg atom, forming an Fe(001)/FeO/MgO interface.

Figures 3(a) and 3(b) show the orbital resolved DOS at the interfacial Fe atom for the clean Fe(001)/MgO and oxidized Fe(001)/FeO/MgO interfaces, respectively. In the latter case, the interfacial Fe atom lies in the FeO plane. For the clean Fe(001)/MgO interface, there is a pronounced peak in the DOS of the interfacial Fe atom just above the Fermi energy. This

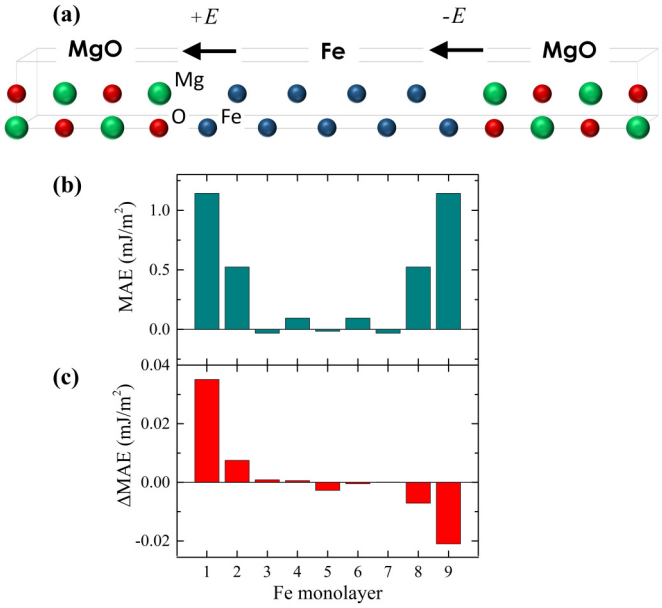

FIG. 2. (a) MgO/Fe/MgO supercell structure (vacuum layer is not shown). (b) and (c) Contributions from different Fe sites (monolayers) to MAE (b) and to the change in MAE (ΔMAE) in applied electric field $E_{\mathrm{vac}} = 2\mathrm{V/nm}$ (c).

peak is associated with the interface resonant state, which is largely composed of the $d_{xz,yz}$ orbitals [Fig. 3(a), bottom panel, blue curve]. The sizable portion of the minority-spin d_{xy} states are occupied for the clean interface [Fig. 3(a), bottom panel, red curve], whereas for the oxidized interface, these states are largely unoccupied and lie in the range of energies from 1 to 3 eV above the Fermi level [Fig. 3(b), bottom panel, red curve]. These are antibonding states resulting from the hybridization of the d_{xy} orbitals of Fe and $p_{x,y}$ orbitals of O in the (001) plane.

In all our calculations, we do not relax the atomic structure in the presence of the electric field. The electric field in the MgO layer is expected to be $E_{\mathrm{MgO}} = E_{\mathrm{vac}}/\varepsilon$, where ε is the dielectric constant of MgO and E_{vac} is the electric field in vacuum. From our calculation, we estimate the dielectric constant to be $\varepsilon \approx 3.3$ from the calculated ratio of potential slope between MgO and vacuum, which is less than the experimental value of $\varepsilon \approx 9.5$ due to neglect of the ionic response of MgO in the calculation. In order to take into account this deficiency, we plot the MAE in Fig. 4 against the expected electric field in MgO corresponding to experimental conditions, i.e., $E_{\mathrm{MgO}} = E_{\mathrm{vac}}/9.5$.

IV. IMPLICATIONS OF THE SIMPLE MODEL

Now we discuss a number of important implications that follow from the simplistic consideration given in Sec. II by comparing it to the results of our DFT calculations. First, it is seen that the largest positive MAE (PMA) occurs for n close to 6, corresponding to Fe. The large PMA does not necessary require hybridization of Fe-d_{z^2} and O-p_z orbitals across the Fe/MgO interface, as is often thought [40,41], and can be explained purely based on the orbital population. In particular, our first principles calculations predict a sufficiently large PMA of about 0.87 mJ/m^2 for the clean Fe (001) surface

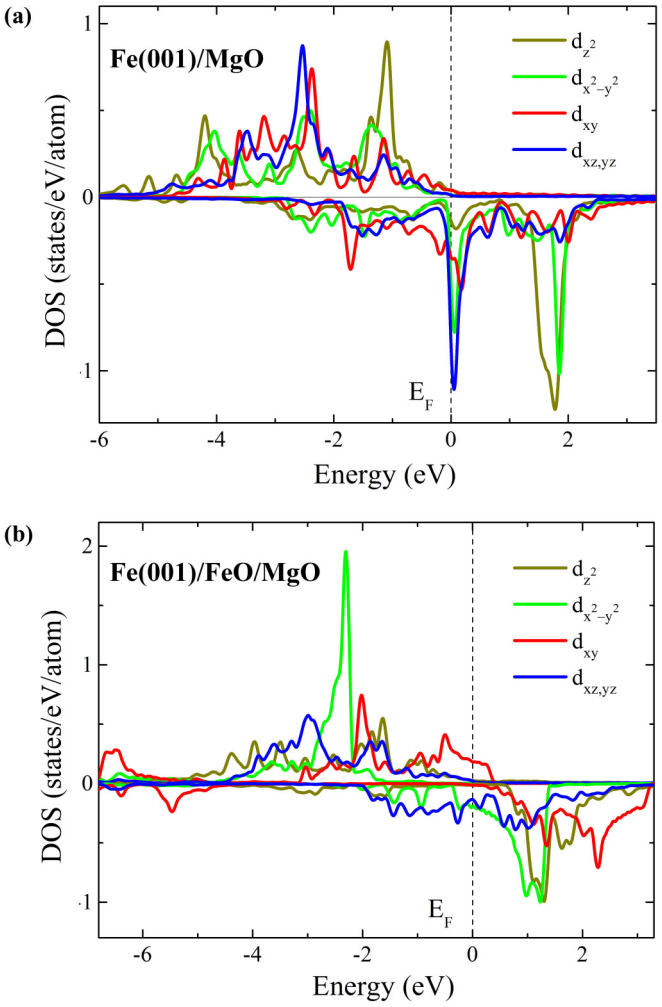

FIG. 3. Orbital resolved DOS at the interfacial Fe atom for clean Fe(001)/MgO (a) and oxidized Fe(001)/FeO/MgO (b) interfaces. Top and bottom panels correspond to majority- and minority-spin contributions, respectively. Fermi energy lies at zero energy, as indicated by the dashed line.

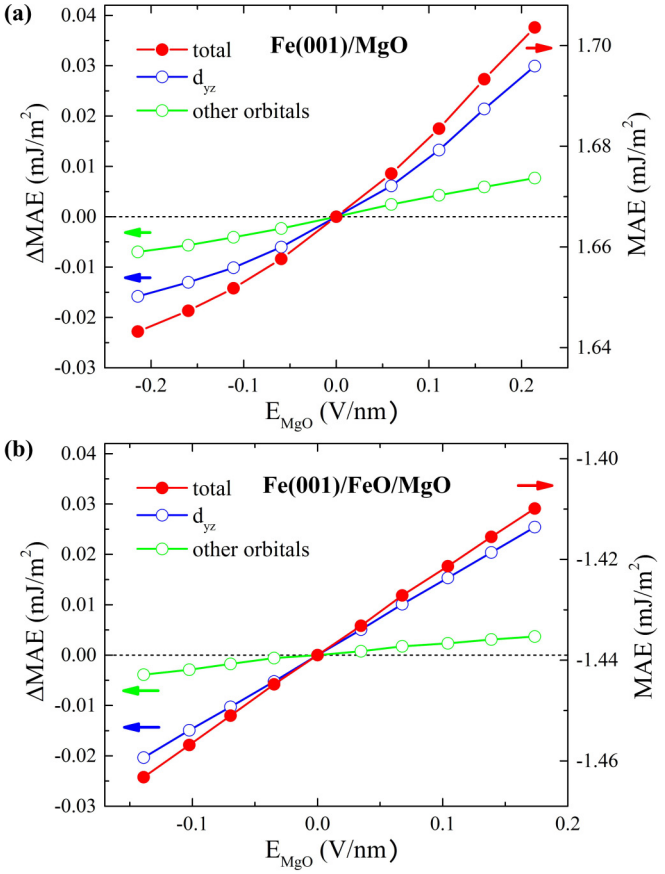

FIG. 4. Results of DFT calculations for Fe(001)/MgO (a) and Fe(001)/FeO/MgO (b) interfaces. MAE as a function of applied electric field E_{MgO} in MgO (red curves) and E field-induced changes in the orbital contribution to MAE (green and blue curves). In the plot, the electric field E_{MgO} is scaled according to the experimental dielectric constant of MgO $\varepsilon = 9.5$.

without MgO. Second, the MAE drops when moving from Fe to Co in terms of the band filling, and it becomes negative for Co. This is consistent with the results of DFT calculations performed for the $Fe_{1-x}Co_x/MgO$ interface as a function of x [42]. Third, since the VCMA is controlled by a change in the $3d$ band population produced by the applied electric field, the slope of the curves in Fig. 1(b) determines the sign of VCMA. It is seen that for n changing from 6 to 7 (i.e., from Fe to Co), the slope is negative, indicating that the MAE decreases with the addition of electrons, which is due to the population of the d_{yz} orbitals. This is consistent with our DFT calculation for the Fe/MgO (001) interface, showing that the MAE increases with the increasing electric field pointing from Fe to MgO (electron depletion), as evident from Fig. 4(a) [43]. The increase of PMA with electron depletion is typical for most of experiments on Fe(Co)/MgO interfaces [17–26] and is known for the clean Fe (001) surface [3]. The dominant contribution comes from the d_{yz} band, which is again consistent with the qualitative picture presented above. Finally, it is notable from Fig. 1(b) that reducing n below 6 leads to the decrease of MAE due to the reduction of the positive contribution involving transitions from the d_{xy} orbital. This changes the sign of VCMA and has important implications, as discussed below.

Furthermore, this simple analysis explains a change in sign of the MAE, when the Fe/MgO interface becomes oxidized. Our calculations predict that the MAE alters from about $+1.67$ mJ/m^2 for the clean Fe/MgO interface to -1.44 mJ/m^2 for the Fe(001)/FeO/MgO interface, where the first monolayer of Fe is fully oxidized [Fig. 4(b)]. This is due to the hybridization of the d_{xy} orbitals of Fe and $p_{x,y}$ orbitals of O in the (001) plane, resulting in the formation of the bonding and antibonding states. The minority-spin antibonding state is largely composed of the d_{xy} orbitals and pushed up in energy, as seen from Fig. 3(b). This behavior is captured by our simple model with negative Δ, which puts the $d_{xz,yz}$ doublet at the lowest energy. In this case, for n changing from 5 to 7, the positive contribution to MAE involving the d_{xy} orbital is eliminated, resulting in the increasing negative contribution coming from the population of the $d_{xz,yz}$ states [Fig. 1(b), blue curves]. Moreover, this qualitative analysis predicts the VCMA sign consistently with our DFT calculation, showing that the MAE increases with the increasing electric field pointing from Fe to MgO and is largely determined by the contribution involving the d_{yz} orbital [Fig. 4(b)].

V. ELECTROSTATIC DOPING

Now we expand these considerations to elucidate the effects of electrostatic and chemical doping on VCMA of the Fe(001)/MgO interface. First, we consider the effect of electrostatic doping, assuming an ultrathin Fe layer that is typical for PMA experiments. A particular calculation is performed in a symmetric geometry of the MgO (3 ML)/Fe (3 ML)/MgO (3 ML)/vacuum (2 nm) supercell. The structure is relaxed for the neutral system until the force on all atoms is less than 1 meV/Å. The MAE is evaluated using the force theorem [44]. Within this approach, first, the electronic structure is self-consistently calculated in the absence of SOC, and then the MAE is obtained by taking the band energy difference for magnetization pointing along the x and z directions in the presence of SOC.

Electrostatic doping is performed by changing the number of valence electrons in the whole system and neutralizing this charge by the background of the constant charge of the opposite sign. By using this method, the excess charge density in vacuum and MgO is redistributed in a way to deposit most of the charge to the metal surface (interface), which is analogous to the electric field effect. The constant charge density background extending to the metal region produces a chemical doping effect, in addition to electrostatic doping through the electric field. This effect is minimized in our calculations due to the sufficiently large supercell (3.91 nm) compared to Fe layer thickness (0.43 nm). Due to the imposed symmetry, the two interfaces in the supercell are exposed to the same field. Atomic relaxations are not performed for the charged system.

Figure 5 shows results of calculation for the excess valence charge $n_e = -0.025$ (the negative number corresponds to adding holes). It is seen that the electrostatic potential in vacuum has a parabolic shape, which is due to a constant background charge in vacuum. The MAE and n_e for the Fe(001)/MgO interface are considered to be half of the corresponding values for the supercell, which contains two identical interfaces. By employing this method, we are able to expose the whole system to excess charge involving both the electric field and the electron/hole doping, in which the electric field is modeled within the linear response regime around the charge neutrality.

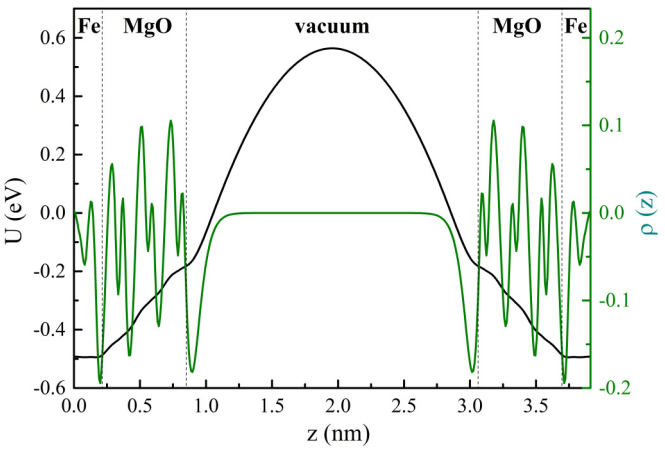

FIG. 5. Calculated electrostatic potential energy (black curve) and excess charge distribution (green curve) across the MgO (3 ML)/Fe (3 ML)/MgO (3 ML)/vacuum (2 nm) supercell structure for $n_e = -0.025$.

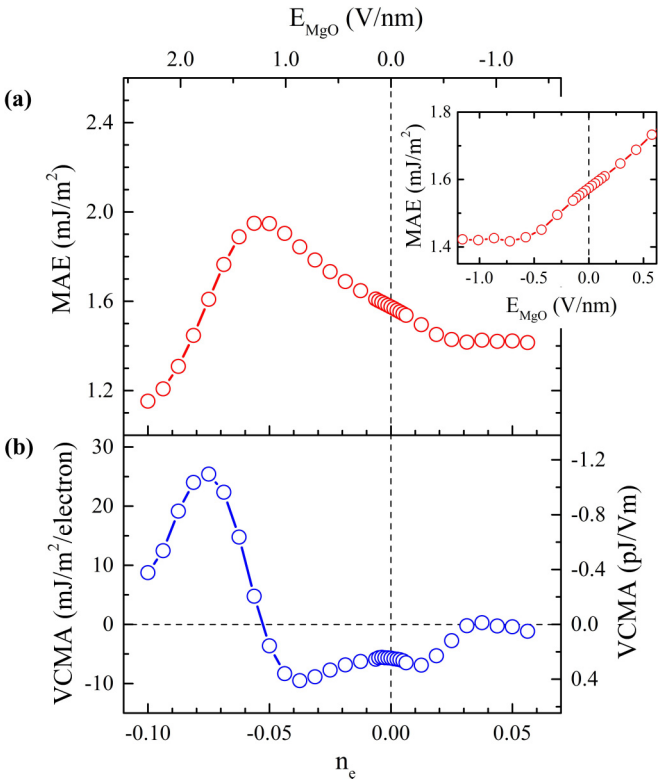

FIG. 6. Calculated MAE (a) and VCMA (b) as a function of the excess number of valence electrons n_e (holes for negative n_e) at the Fe(001)/MgO interface. The inset shows the MAE as a function of the electric field in MgO. The electric field is estimated from $E_{\mathrm{MgO}} = n_e/\varepsilon\varepsilon_0 a^2$. The positive field is assumed to be pointing from Fe to MgO and corresponds to electron depletion [45].

The results of the calculation are shown in Fig. 6(a), where MAE is plotted against the excess valence charge n_e. For $n_e = 0$, we find that MAE is about 1.57 mJ/m^2. It increases as holes are added to the system corresponding to an increasing electric field pointing from Fe to MgO. This behavior is consistent with previous calculations [6] and typical for experiments [17–20]. For small values of n_e, the MAE changes linearly with n_e. The slope of the curve determines VCMA, which is shown in Fig. 6(b). Assuming that the electric field in MgO is given by $E_{\mathrm{MgO}} = -n_e/\varepsilon\varepsilon_0 a^2$, where ε is the dielectric constant of MgO, ε_0 is the vacuum permittivity and a is the in-plane lattice parameter, we find a VCMA of about 0.25 pJ/Vm. This value is comparable to that in Fig. 4(a) (∼0.15 pJ/Vm). With increasing n_e up to about 0.025($E_{\mathrm{MgO}} \approx -0.5$ V/nm) the MAE curve becomes flatter [Fig. 4(a)], and with $n_e \approx 0.03$, the VCMA is reduced. Such a nonlinear variation of MAE [Fig. 6(a), inset] has been seen in a number of experiments [18,20]. This behavior can be attributed to the resonant minority-spin interface state, which is well known from spin-polarized tunneling [46]. In our calculation, the interface state appears around 0.05 eV above the Fermi energy and is largely composed of the $d_{xz,yz}$ orbitals [Fig. 3(a)].

According to Plucinski *et al.* [47], this state lies in the energy gap of the projected minority-spin bulk bands. Thus, electric field-induced occupation of this state does not lead to a sizable reduction in the MAE (as expected for the d_{yz} orbital) due to the absence of the unoccupied counterpart E_g states to affect the MAE through $\langle d_{yz}|L_x|d_{z^2}\rangle$ and $\langle d_{yz}|L_x|d_{x^2-y^2}\rangle$ matrix elements. The energy position of the resonant state is sensitive both to the approximations used in the calculation (within the range ~0.1 eV) and to the structural defects in grown samples, such as oxygen vacancies and interface oxidation. This may shift the flat region in the MAE curve [Fig. 6(a), inset] closer to the zero field, as has been observed experimentally [18,20].

However, the most striking feature that is evident from Fig. 6 is the maximum in MAE at $n_e \approx -0.05$ and a change of VCMA sign at $n_e < -0.05$. This behavior is consistent with our simple analysis, according to which the inverse VCMA occurs when $n < 6$ due to the reduced contribution from the d_{xy} orbitals [Fig. 1(b), red lines]. In this inverse regime, the VCMA reaches a very large negative value of about -1.1 pJ/Vm at $n_e = -0.075$. This regime may be achieved by charge transfer or alloying, as we discuss below. Realizing this regime experimentally may be favorable for the practical purpose of voltage-driven magnetization reversal.

The inverse VCMA may be achieved through the electrostatic doping caused by a top metal layer covering the PMA ferromagnet. Due to the different work functions of the PMA ferromagnet and the adjacent metal layer, charge transfer occurs between the layers to equalize the chemical potentials, changing the number of valence electrons in the ferromagnetic metal. The effect may be sizable only for ultrathin magnetic films due to the short screening length in metals. This may explain the results of Shiota *et al.* [26], who observed a change of VCMA from normal to inverse, when the Ta underlayer was replaced with Ru in the M/CoFeB/MgO (M = Ta,Ru) multilayer. The work function of Ta is about 0.25 eV lower than that of Fe, whereas the work function of Ru is 0.21 eV higher [48]. Therefore, it is expected that Fe is electron doped at the interface with Ta but hole doped at the interface with Ru, which may lead to the inverse VCMA. Also, the results of Nozaki *et al.* [20] demonstrate that VCMA is enhanced up to 0.29 pJ/Vm when a subnanometer-thick layer of Fe is interfaced with Cr. At such a small thickness, the effects of intermixing may play a role, resulting in the hole doping of Fe. According to Fig. 6(b), small hole doping raises VCMA up to about 0.4 pJ/Vm (at $n_e = -0.04$), which may be the origin of the enhanced VCMA observed by Nozaki *et al.* [20]. The effect of capping or interface layers may involve additional effects, such as interface hybridization [7,14] and quantum well states [12,49,50]. Here, however, we only emphasize the importance of the charge transfer as the mechanism controlling VCMA.

VI. CHEMICAL DOPING

Chemical doping is another way to manipulate VCMA. Here, we consider effects of Fe alloyed with Co or Cr. Doping with Co adds electrons to Fe, whereas doping with Cr adds holes. This is expected to have an opposite effect on the MAE of the $Fe_{1-x}M_x$/MgO (M = Co,Cr) interface, according to the simple analysis of Fig. 1(b).

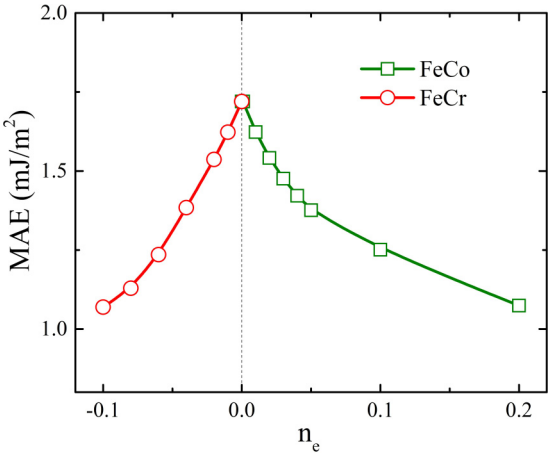

FIG. 7. MAE of the $Fe_{1-x}M_x$/MgO interface (M = Co,Cr) versus a number of doped electrons n_e (holes for negative n_e) calculated by the KKR-CPA method.

Calculations are performed using the full relativistic screened Korringa-Kohn-Rostoker (KKR) method based on DFT, where the SOC is taken into account by solving the full relativistic Dirac equation [51]. The coherent potential approximation (CPA) is utilized to describe the compositional dependence of the $Fe_{1-x}M_x$ alloys. The potentials are described within the atomic sphere approximation (ASA). Particular calculations are performed using $Fe_{1-x}M_x$ (3 ML)/MgO (3 ML) supercell geometry by imposing periodic boundary conditions. A reference value of the MAE calculated by the KKR-CPA method for the Fe/MgO interface is about 1.72 mJ/m^2, which is in good agreement with the value calculated by VASP (1.57 mJ/m^2). More details of the calculations can be found in Ref. [42].

The results are shown in Fig. 7, where the MAE is plotted against the number of doped electrons (holes), assuming that $n_e = x$ for Co and $n_e = 1 - 2x$ for Cr. In agreement with the published results [42], the MAE is decreasing when adding electrons to Fe (FeCo/MgO). However, when Fe is doped with holes (FeCr/MgO), the MAE is decreasing. This is consistent with our expectation, though a simple picture of doping fails at a very small doping level at which, according to Fig. 6, we saw an increase of MAE in the range of n_e down to -0.05. This discrepancy indicates that doping with Cr is not the same as the rigid decrease of the number of electrons in Fe. Nevertheless, we see again a qualitative agreement between our simple picture presented in Fig. 1(b) and the accurate calculation shown in Fig. 7.

VII. SUMMARY

In conclusion, starting from a simple picture of orbital population, we have qualitatively explained the available results of the voltage-controlled surface (interface) magnetic anisotropy of 3d transition-metal thin films used in MTJs. The results of the DFT calculations for the Fe (001) surface, clean $Fe_{1-x}Co_x$(001)/MgO interface, and oxidized Fe(001)/MgO interface, involving effects of alloying and the electric field, can be understood in terms of changes in the population of the minority-spin $d_{xz,yz}$ orbitals, which enhance

the surface MAE with electron depletion at the interface. However, the hole-doped Fe(001) exhibits an inverse VCMA, where the MCA enhancement is achieved when electrons are accumulated at the Fe(001)/MgO interface. In this regime, we predict a significantly enhanced VCMA that exceeds 1 pJ/Vm. These results may be important to find the material structures with enhanced VCMA, which is critical for device applications.

ACKNOWLEDGMENTS

This research was supported by the Nanoelectronics Research Corporation (NERC), a wholly owned subsidiary of the Semiconductor Research Corporation (SRC), through the Center for Nanoferroic Devices (CNFD). Computations were performed at the University of Nebraska Holland Computing Center.

[1] F. Matsukura, Y. Tokura, and H. Ohno, Nat. Nanotech. **10**, 209 (2015).
[2] E. Y. Tsymbal, Nat. Mater. **11**, 12 (2012).
[3] C.-G. Duan, J. P. Velev, R. F. Sabirianov, Z. Zhu, J. Chu, S. S. Jaswal, and E. Y. Tsymbal, Phys. Rev. Lett. **101**, 137201 (2008).
[4] H. Zhang, M. Richter, K. Koepernik, I. Opahle, F. Tasnádi, and H. Eschrig, New J. Phys. **11**, 043007 (2009).
[5] K. Nakamura, R. Shimabukuro, Y. Fujiwara, T. Akiyama, T. Ito, and A. J. Freeman, Phys. Rev. Lett. **102**, 187201 (2009).
[6] K. Nakamura, T. Akiyama, T. Ito, M. Weinert, and A. J. Freeman, Phys. Rev. B **81**, 220409(R) (2010).
[7] M. Tsujikawa and T. Oda, Phys. Rev. Lett. **102**, 247203 (2009).
[8] M. K. Niranjan, C.-G. Duan, S. S. Jaswal, and E. Y. Tsymbal, Appl. Phys. Lett. **96**, 222504 (2010).
[9] P. Lukashev, J. D. Burton, S. S. Jaswal, and E. Y. Tsymbal, J. Phys.: Condens. Matter **24**, 226003 (2012).
[10] S. Suzuki, S. Yasuda, K. Edakawa, and S. Seki, J. Phys. Soc. Jpn. **82**, 124715 (2013).
[11] P. Ruiz-Díaz, T. R. Dasa, and V. S. Stepanyuk, Phys. Rev. Lett. **110**, 267203 (2013).
[12] P. V. Ong, N. Kioussis, P. K. Amiri, J. G. Alzate, K. L. Wang, G. P. Carman, J. Hu, and R. Wu, Phys. Rev. B **89**, 094422 (2014).
[13] O. O. Brovko, P. Ruiz-Díaz, T. R. Dasa, and V. S. Stepanyuk, J. Phys.: Condens. Matter **26**, 093001 (2014).
[14] P. V. Ong, N. Kioussis, D. Odkhuu, P. K. Amiri, K. L. Wang, and G. P. Carman, Phys. Rev. B **92**, 020407(R) (2015).
[15] F. Ibrahim, H. X. Yang, A. Hallal, B. Dieny, and M. Chshiev, Phys. Rev. B **93**, 014429 (2016).
[16] M. Weisheit, S. Fähler, A. Marty, Y. Souche, C. Poinsignon, and D. Givord, Science **315**, 349 (2007).
[17] T. Maruyama, Y. Shiota, T. Nozaki, K. Ohta, N. Toda, M. Mizuguchi, A. A. Tulapurkar, T. Shinjo, M. Shiraishi, S. Mizukami, Y. Ando, and Y. Suzuki, Nat. Nanotech. **4**, 158 (2009).
[18] A. Rajanikanth, T. Hauet, F. Montaigne, S. Mangin, and S. Andrieu, Appl. Phys. Lett. **103**, 062402 (2013).
[19] S. Miwa, K. Matsuda, K. Tanaka, Y. Kotani, M. Goto, T. Nakamura, and Y. Suzuki, Appl. Phys. Lett. **107**, 162402 (2015).
[20] T. Nozaki, A. Kozioł-Rachwał, W. Skowroński, V. Zayets, Y. Shiota, S. Tamaru, H. Kubota, A. Fukushima, S. Yuasa, and Y. Suzuki, Phys. Rev. Appl. **5**, 044006 (2016).
[21] Y. Shiota, T. Maruyama, T. Nozaki, T. Shinjo, M. Shiraishi, and Y. Suzuki, Appl. Phys. Exp. **2**, 063001 (2009).
[22] T. Nozaki, Y. Shiota, M. Shiraishi, T. Shinjo, and Y. Suzuki, Appl. Phys. Lett. **96**, 022506 (2010).
[23] S. Kanai, M. Yamanouchi, S. Ikeda, Y. Nakatani, F. Matsukura, and H. Ohno, Appl. Phys. Lett. **101**, 122403 (2012).
[24] W.-G. Wang, M. Li, S. Hageman, and C. L. Chien, Nat. Mater. **11**, 64 (2012).
[25] Y. Shiota, T. Nozaki, F. Bonell, S. Murakami, T. Shinjo, and Y. Suzuki, Nat. Mater. **11**, 39 (2012).
[26] Y. Shiota, F. Bonell, S. Miwa, N. Mizuochi, T. Shinjo, and Y. Suzuki, Appl. Phys. Lett. **103**, 082410 (2013).
[27] C. Bi, Y. Liu, T. Newhouse-Illige, M. Xu, M. Rosales, J. W. Freeland, O. Mryasov, S. Zhang, S. G. E. te Velthuis, and W. G. Wang, Phys. Rev. Lett. **113**, 267202 (2014).
[28] U. Bauer, L. Yao, A. J. Tan, P. Agrawal, S. Emori, H. L. Tuller, S. Dijken, and G. S. D. Beach, Nat. Mater. **14**, 174 (2015).
[29] G. Van der Laan, J. Phys.: Condens. Matter **10**, 3239 (1998).
[30] P. Bruno, Phys. Rev. B **39**, 865 (1989).
[31] The specific role of the d_{yz} orbital in the $d_{xz,yz}$ manifold comes from our choice of the x axis to define the MAE in Eq. (1).
[32] P. E. Blöchl, Phys. Rev. B **50**, 17953 (1994).
[33] G. Kresse and D. Joubert, Phys. Rev. B **59**, 1758 (1999).
[34] J. P. Perdew, K. Burke, and M. Ernzerhof, Phys. Rev. Lett. **77**, 3865 (1996).
[35] M. Methfessel and A. T. Paxton, Phys. Rev. B **40**, 3616 (1989).
[36] We do not relax the atomic positions in the presence of the electric field. The electric field-induced atomic displacements in MgO are responsible for the ionic contribution to the dielectric constant and produce an additional effect on MAE. We take these into account by scaling the electric field in MgO to the experimentally measured value of the dielectric constant $\varepsilon = 9.5$.
[37] G. Kresse and O. Lebacq, *VASP Manual*, http://cms.mpi.univie.ac.at/vasp/.
[38] V. Antropov, L. Ke, and D. Aberg, Solid State Comm. **194**, 35 (2014).
[39] J. Neugebauer and M. Scheffler, Phys. Rev. B **46**, 16067 (1992).
[40] H. X. Yang, M. Chshiev, B. Dieny, J. H. Lee, A. Manchon, and K. H. Shin, Phys. Rev. B **84**, 054401 (2011).
[41] J. Okabayashi, J. W. Koo, H. Sukegawa, S. Mitani, Y. Takagi, and T. Yokoyama, Appl. Phys. Lett. **105**, 122408 (2014).
[42] J. Zhang, C. Franz, M. Czerner, and C. Heiliger, Phys. Rev. B **90**, 184409 (2014).
[43] The VCMA sign is opposite that in Ref. [8] due to incorrect assignment of the electric field orientation given in that paper when calculating the MAE.
[44] A. Lehnert, S. Dennler, P. Błoński, S. Rusponi, M. Etzkorn, G. Moulas, P. Bencok, P. Gambardella, H. Brune, and J. Hafner, Phys. Rev. B **82**, 094409 (2010).
[45] The whole electric field range indicated in Fig. 6 may not be accessible in practice because it exceeds the breakdown voltage of MgO.
[46] K. D. Belashchenko, J. Velev, and E. Y. Tsymbal, Phys. Rev. B **72**, 140404(R) (2005).
[47] L. Plucinski, Y. Zhao, C. M. Schneider, B. Sinkovic, and E. Vescovo, Phys. Rev. B **80**, 184430 (2009).

[48] H. B. Michaelson, J. Appl. Phys. **48**, 4729 (1977).
[49] M. Przybylski, M. Dąbrowski, U. Bauer, M. Cinal, and J. Kirschner, J. Appl. Phys. **111**, 07C102 (2012).
[50] M. Cinal and D. M. Edwards, Phys. Rev. B **57**, 100 (1998).
[51] J. Zabloudil, R. Hammerling, L. Szunyogh, and P. Weinberger, *Electron Scattering in Solid Matter: A Theoretical and Computational Treatise, Springer Series in Solid-State Sciences* (Springer, Berlin, 2005), Vol. 147.